Sn-Doped Rutile TiO$_2$ Hollow Nanocrystals with Enhanced Lithium-Ion Batteries Performance

Shilong Jiao,[†,∥] Gang Lian,*[†,□,∥] Laiying Jing,[†] Zhenghao Xu,[†] Qilong Wang,[‡] Deliang Cui,*[†] and Ching-Ping Wong,*[□]

† State Key Lab of Crystal Materials, Shandong University, Jinan 250100, P. R. China

‡ Key Laboratory for Special Functional Aggregated Materials of Education Ministry, School of Chemistry & Chemical Engineering, Shandong University, Jinan 250100, P. R. China

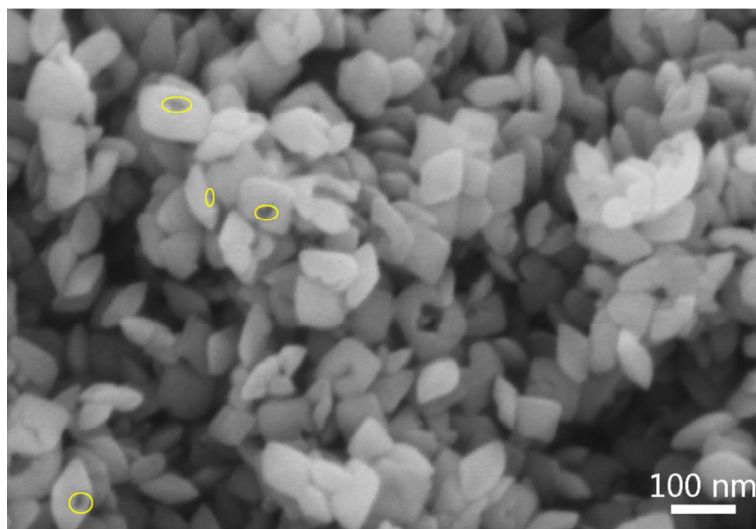□School of Materials Science and Engineering, Georgia Institute of Technology, Atlanta, Georgia 30332, United State

E-mail: liangang@sdu.edu.cn, cuidl@sdu.edu.cn, cpwong@cuhk.edu.hk
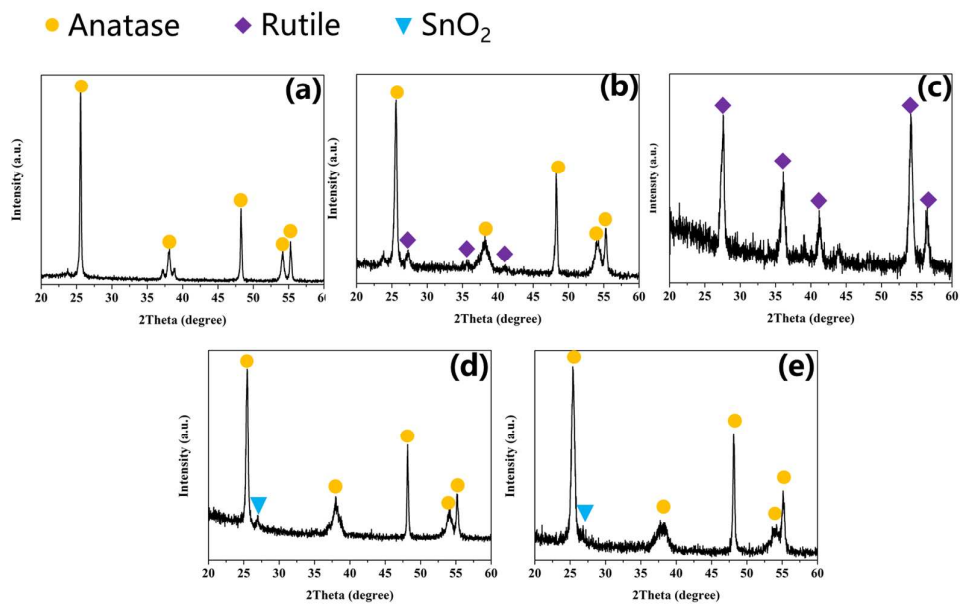
Supporting Information Contents

-Figures S1.-S14.

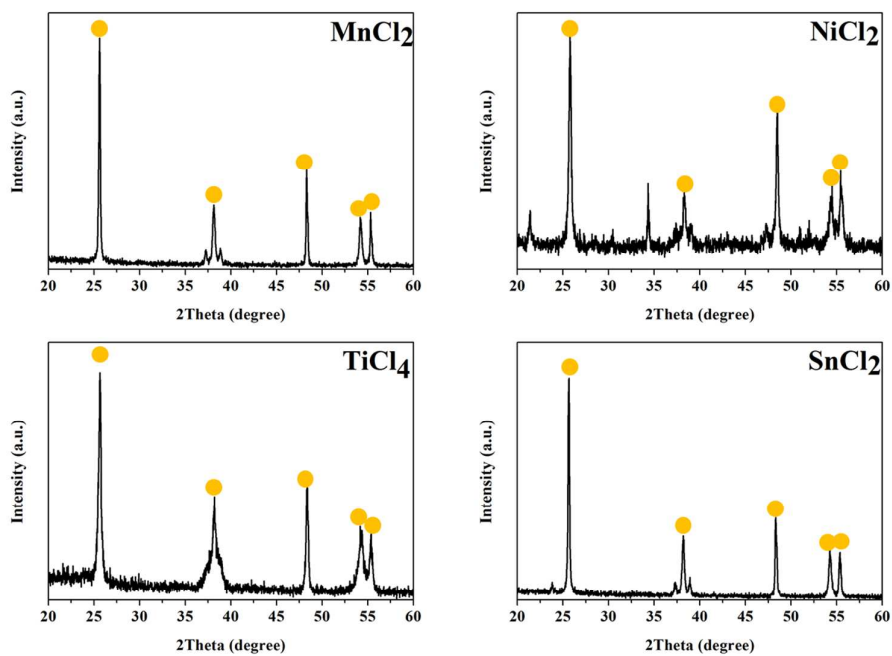-Supporting Information Table S1. and Table S2.

-References

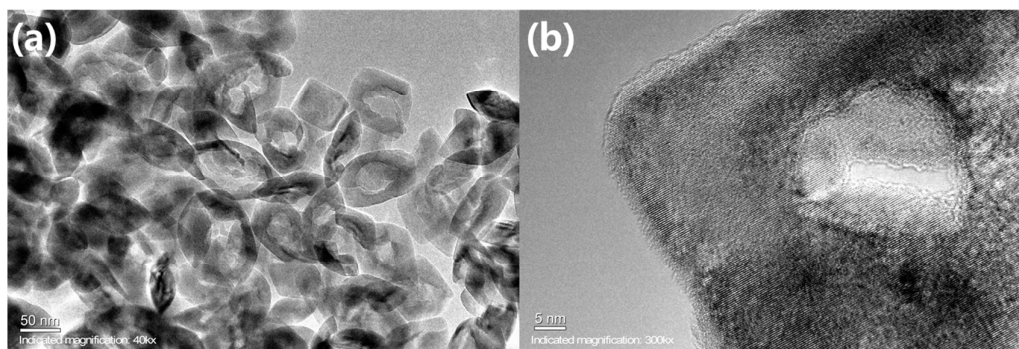**Figure S1.** SEM image of the as-obtained Sn-doped rutile TiO_2 hollow nanocrystals.

Figure S2. XRD patterns of the as-obtained TiO_2 synthesized with (a) 0 mmol, (b) 2 mmol, (c) 4 mmol, (d) 6 mmol and (e) 8 mmol $SnCl_4 \cdot 5H_2O$.
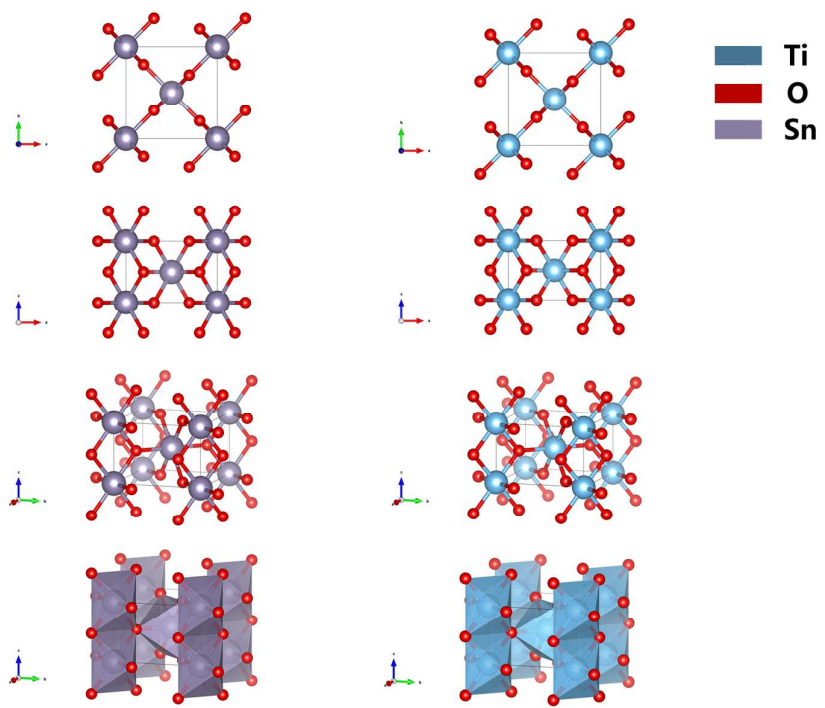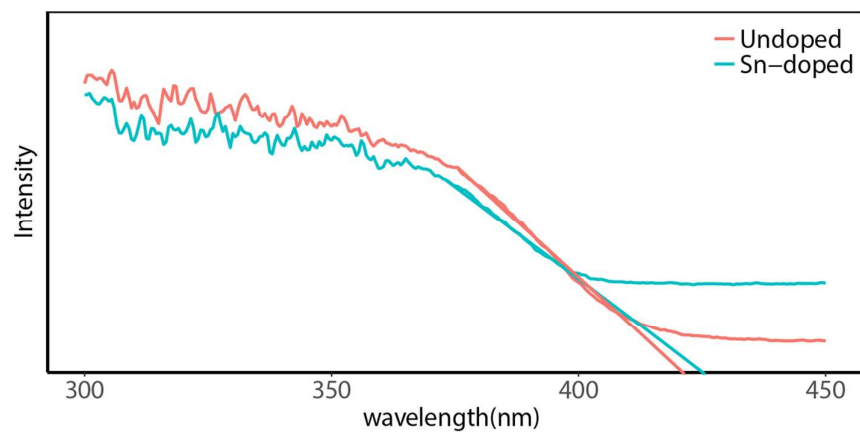
Figure S1. The XRD patterns of the products synthesized with other metal chlorides while keeping the molar amount of Cl⁻ same with the $SnCl_4$ reaction system.

Figure S4. (a) TEM and (b) HRTEM images of the as-obtained Sn-doped rutile TiO_2

hollow nanocrystals.

**Figure S5.** Schematic illustrations of SnO_2 and rutile TiO_2.

Figure S6. UV-vis spectra of the Sn-doped rutile TiO_2 hollow nanocrystals and the un-doped rutile TiO_2. The calculated band gap of Sn-doped TiO_2 is ~2.9 eV, which is slightly lower than the pure rutile TiO_2. DFT-based theoretical calculations shows that the doping of tin acts as the main reason for the decrease of the bandgap.
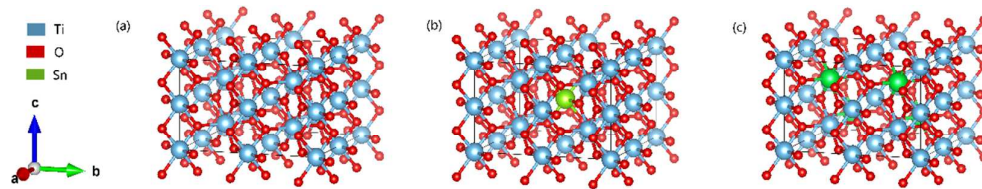
Figure S7. Schematic illustration of initial structures for the Sn-doped rutile TiO_2 with different doping amount. (a) pure rutile TiO_2, (b) 6.25% Sn-doped rutile TiO_2, (c) 25% Sn-doped rutile TiO_2.

DFT-based (density functional theory) simulation was run using Dmol^3 package in the Materials Studio Software. A 2*2*2 supercell was created by replication of the elementary cell in the x, y, z directions. Generalized gradient approximation (GGA) functional proposed by Perdew−Burke−Ernzerhof [1-3](PBE) was used. DSPP (DFT Semi-core Pseudopotential) was used to describe the electron and core interaction. A global cutoff of 5 Å was used which is the same setting for all the models.
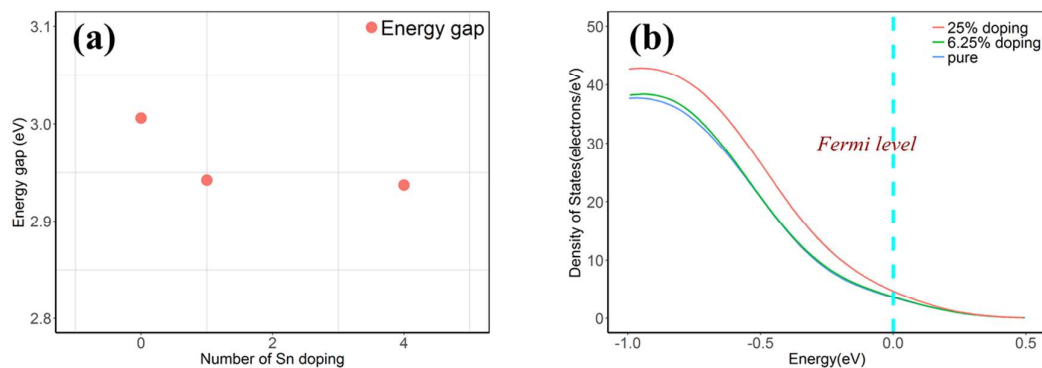
Figure S8. (a) Relationship between the energy gap and the number of Sn doping. (b) DOS spectra of the three different systems.

The calculated bandgaps were 3.006 eV for pure rutile TiO_2, 2.942 eV for 6.25% Sn-doped rutile TiO_2, and 2.937 eV for 25% Sn-doped rutile TiO_2. The results indicate that the bandgap narrows with increasing the amount of Sn in rutile TiO_2. Further analysis of the electron states distribution shows that the density of states near the Fermi level increases with the amount of Sn, which is beneficial for the photo-related catalysis or energy transformation process.
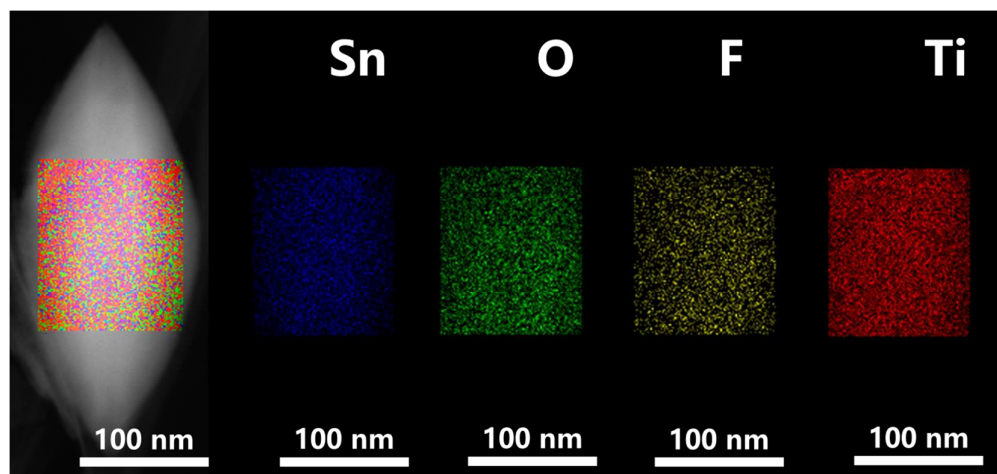
Figure S9 STEM image of single Sn-doped $TiOF_2$ nanocrystal and EDS mappings of Sn, O, F and Ti elements.
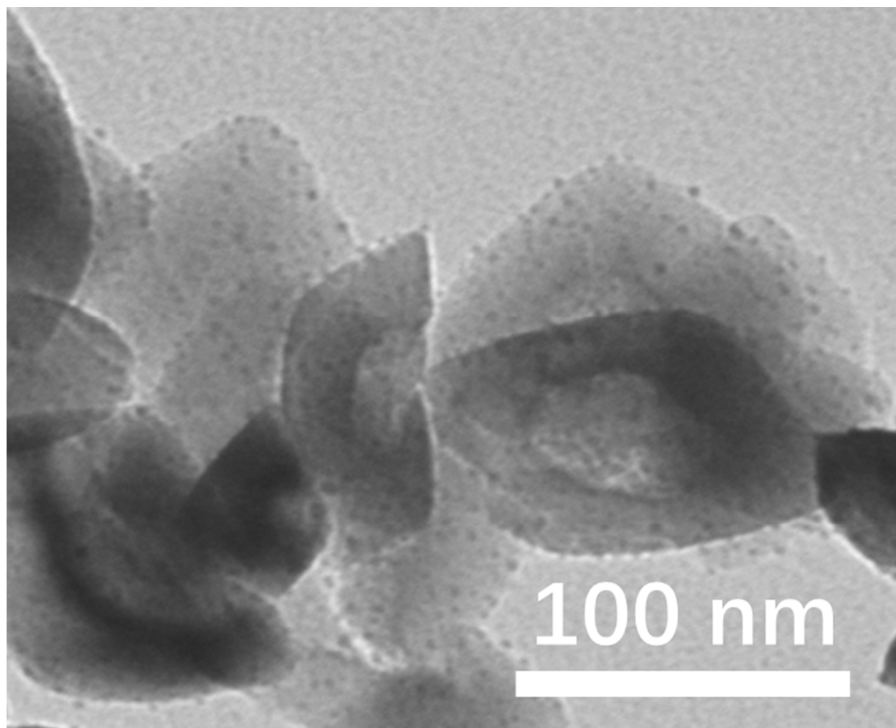
Figure S10. TEM image of the rutile Sn-doped TiO_2 nanocrystals on the surfaces of solid Sn-doped $TiOF_2$.
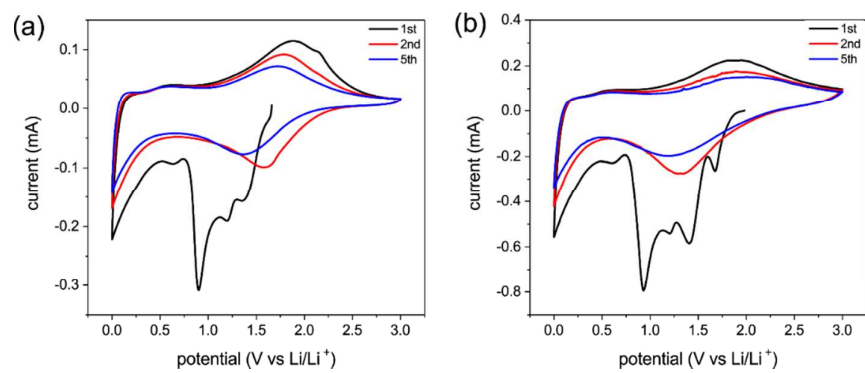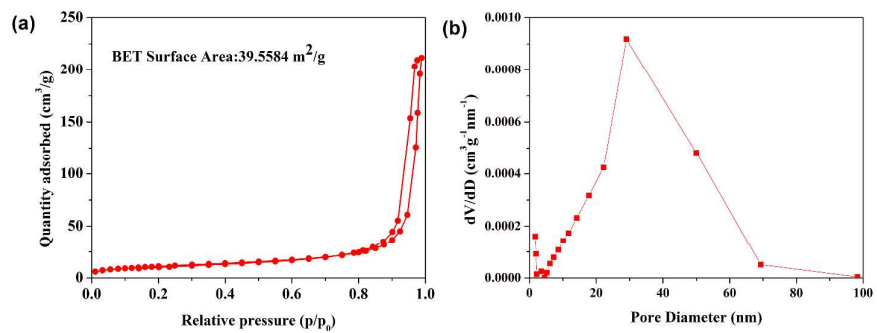
Figure S11. CV profiles of (a) un-annealed and (b) annealed Sn-doped rutile TiO_2 hollow nanocrystals showing the 1st, 2nd and 5th cycles between 0.01 and 3.0 V at a scan rate of 0.2 mV s^{-1}.

Figure S12 (a) The nitrogen adsorption/desorption isotherms and (b) the pore size distribution curves of the Sn-doped rutile TiO$_2$ nanocrystals. The BET specific surface area and BJH pore volume are39.5584 m^2/g and 0.32852 cm^3/g .
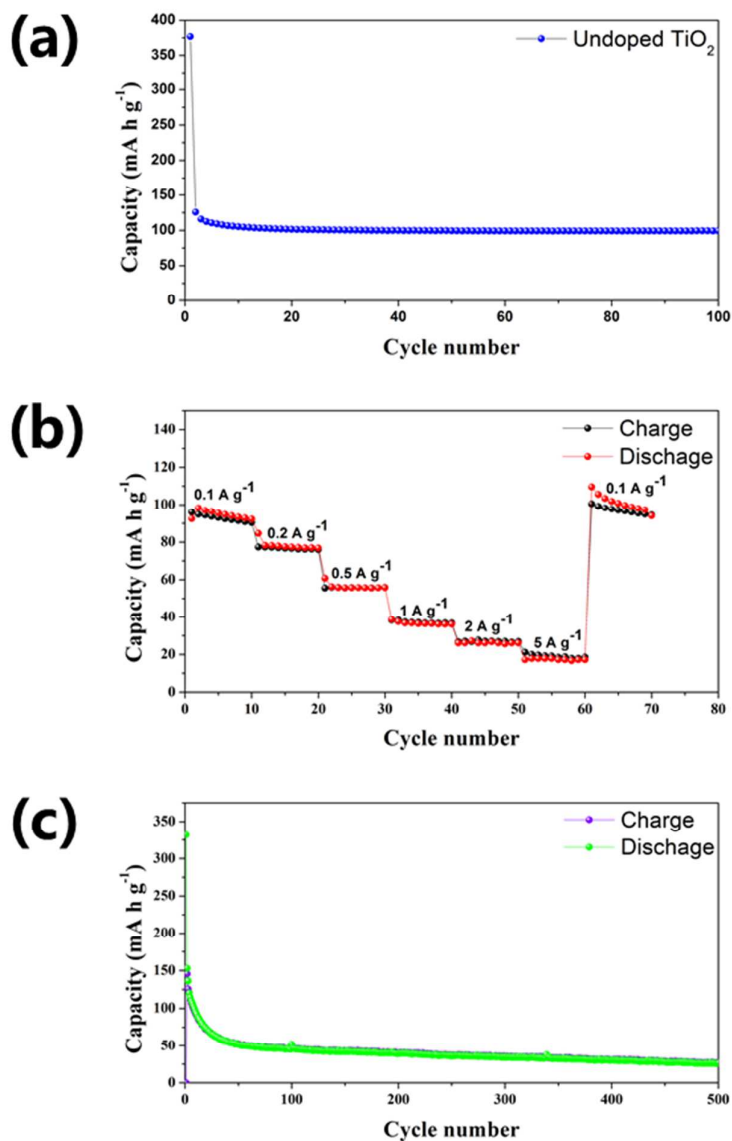
Figure S13. (a) Cycle performance at 100 mA g^{-1} in the 0.01-3 V range of the un-doped TiO$_2$; (b) Rate capabilities of the un-doped TiO$_2$ at a current density ranging from 100-5000 mA h g^{-1}; (c) The cycling performance of annealed Sn-doped rutile TiO$_2$ at the rate of 1000 mA h g^{-1}.
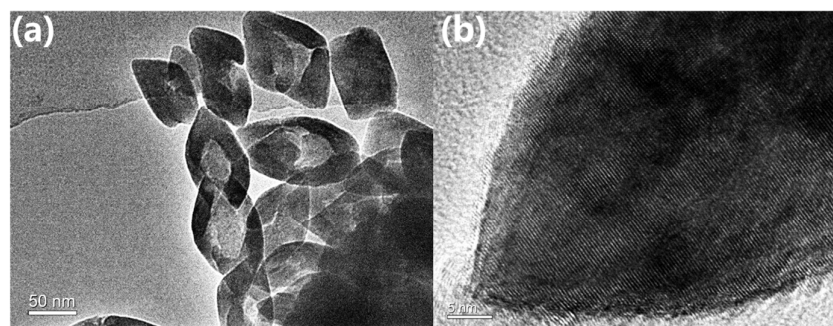
Figure S14 TEM (a) and HRTEM (b) images of the Sn-doped rutile TiO_2 after cycle performance test (1 A g^{-1}, 100 cycles).

Table S1. Comparison of the lattice parameters of rutile SnO_2 and TiO_2.

Material	Rutile SnO_2	Rutile TiO_2
a (Å)	4.73730	4.59400
b (Å)	4.73730	4.59400
c (Å)	3.18640	2.95900
α	90	90
β	90	90
γ	90	90
Space Group	P42/mnm	P42/mnm

Table S2. Comparison of the electrochemical performances of the as-prepared Sn-doped rutile TiO_2 with the reported performances of rutile TiO_2 as anode materials in the LIBs.

Materials	Current rate	Reversible capacity (mA h g^{-1})	Current rate	Reversible capability (mA h g^{-1})
TiO_2 submicroboxes[4]	30 C	68	1C	210
Dark TiO_2 nanorod[5]	50 C	93.6	1 C	166.7
TiO_2 mesocrystals[6]	5 C	100	1 C	171.3
Nanosized TiO_2[7]	30 C	70	1 C	132
TiO_2 microspheres[8]	10 C	106	1 C	160.4
B-doped TiO_2[9]	10 C	72	1 C	154
Sn-doped rutile TiO_2 hollow structure (This work)	**5000 mA g^{-1} (30C)**	**110**	**100 mA g^{-1} (~0.6 C)**	**251**

References

(1)   Perdew, J. P.; Wang, Y.; Pair-distribution function and its coupling-constant average for the spin-polarized electron gas. *Phys. Rev. B* **1992**, *46* (20), 947–954.

(2)   Perdew, J. P. Density-Functional Approximation for the Correlation Energy of the Inhomogeneous Electron Gas. *Phys. Rev. B* **1986**, *33* (12), 8822–8824.

(3)   Perdew, J. P.; Burke, K.; Ernzerhof, M. Generalized Gradient Approximation Made Simple. *Phys. Rev. Lett.* **1996**, *77* (18), 3865–3868.

(4)   Yu, X.-Y.; Wu, H. Bin; Yu, L.; Ma, F.-X.; Lou, X. W. D. Rutile TiO_2 Submicroboxes with Superior Lithium Storage Properties. *Angew. Chemie Int. Ed.* **2015**, *54* (13), 4001–4004.

(5)   Chen, J.; Song, W.; Hou, H.; Zhang, Y.; Jing, M.; Jia, X.; Ji, X. Ti^{3+} Self-Doped Dark Rutile TiO_2 Ultrafine Nanorods with Durable High-Rate Capability for Lithium-Ion Batteries. *Adv. Funct. Mater.* **2015**, 6793–6801.

(6)   Hong, Z.; Wei, M.; Lan, T.; Jiang, L.; Cao, G. Additive-Free Synthesis of Unique TiO_2 Mesocrystals with Enhanced Lithium-Ion Intercalation Properties. *Energy Environ. Sci.* **2012**, *5* (1), 5408.

(7)   Hu, Y. S.; Kienle, L.; Guo, Y. G.; Maier, J. High Lithium Electroactivity of Nanometer-Sized Rutile TiO_2. *Adv. Mater.* **2006**, *18* (11), 1421–1426.

(8) Lan, T.; Liu, Y.; Dou, J.; Hong, Z.; Wei, M. Hierarchically Porous TiO_2 Microspheres as a High Performance Anode for Lithium-Ion Batteries. *J. Mater. Chem. A* **2014**, *2* (4), 1102–1106.

(9) Tian, H.; Xin, F.; Tan, X.; Han, W. High Lithium Electroactivity of Boron-Doped Hierarchical Rutile Submicrosphere TiO_2. *J. Mater. Chem. A* **2014**, *2* (27), 10599–10606.